# Elastic differential cross sections for electron scattering from $SF_6$ and $CS_2$

K. G. Bhushan,* K. C. Rao, S. C. Gadkari, J. V. Yakhmi, and S. K. Gupta
*Technical Physics and Prototype Engineering Division, Bhabha Atomic Research Centre, Mumbai 400 085. India*
(Received 23 October 2008; published 7 January 2009)

Elastic differential cross sections have been measured for electron-$SF_6$ and electron-$CS_2$ collisions in the energy range from 30 eV to 500 eV using a high resolution electron spectrometer. The measured cross sections have been put on an absolute scale using the relative flow technique. The total and momentum transfer cross sections have been determined by extrapolating the differential cross-section data using a least-squares fitting procedure based on standard Legendre polynomial expansion. The measured data are compared with theoretical and other experimental data wherever available. It is seen that the theoretical calculations based on independent-atom-model without polarization potential overestimates the cross sections at lower energies while at higher energies the model seems to be describing the interaction effects adequately.

DOI: 10.1103/PhysRevA.79.012702 PACS number(s): 34.80.Bm, 34.10.+x

## I. INTRODUCTION

It is well known that the measurement of elastic and inelastic differential cross sections for electron-molecule collisions provides detailed information into the nature of electron-target interaction, the initial and final state wave functions, charge and momentum densities and so on [1–3]. Further, measurements of the angular distribution of scattered electrons especially in the low- and intermediate-energy domain (50 eV–500 eV) provide a stringent test for the first-order many-body calculations like the independent atom model (IAM) formalism.

Electron scattering from $SF_6$ is interesting for several reasons; $SF_6$ has a large cross section for the formation of $SF_6^-$ at near zero energies [4]. This feature makes it a gaseous dielectric where high voltage breakdown is averted by removing low-energy electrons as $SF_6^-$. $SF_6$ is also used in dry-etching processes in the semiconductor industry due to its anisotropic and highly directional etch profiles required for submicron level very-large-scale integration (VLSI) circuits [5,6]. Modeling these processes require a better understanding of the electron transport phenomena and electron-impact cross sections. Very- and low-energy (0.05 to 10 eV) elastic differential cross-section measurements have been made by Rohr [7] and Srivastava *et al.* (5–75 eV) [8]. Later, Johnstone and Newell presented absolute differential cross sections (DCS) in the same energy range [9]. In the intermediate energies (75–700 eV) the only work presented is that of Sakae *et al.* [10]. The most recent measurements at low energies (2.7–75 eV) by Cho *et al.*, utilizes a magnetic angle changing device for measuring DCS well into the backward angles [11]. The cross-section data from $SF_6$ generated from the present experiment is mainly used to calibrate our instrument in this study.

$CS_2$ on the other hand, is part of the set of linear triatomic molecules $CS_2$, $CO_2$, and OCS. It is especially interesting since they have similar electronic ground-state configurations and strong dipole polarizabilites [12,13]. While $CO_2$ and OCS have been well studied especially in the intermediate-energy regime, DCS measurements on elastic scattering of electrons from $CS_2$, have been far and few. Sohn *et al.*, [14] have measured absolute vibrationally elastic differential cross sections using a crossed beam setup in the 0.3–5.0 eV range. Total cross section (elastic plus inelastic) measurements up to 100 eV have been reported by Szmytkowski [15]. On the theoretical side, Lee *et al.* [16] have calculated differential and total cross sections up to 100 eV, while Raj and Tomar [17] have used a modified independent atom model to calculate cross sections for energies above 100 eV. To the best of our knowledge, there have been no measurements so far on elastic scattering of electrons from $CS_2$ in this intermediate-energy regime (30 eV–500 eV).

In this paper we report on the measurements of absolute differential cross sections for elastic scattering electrons from $SF_6$ and $CS_2$ in the intermediate-energy region using a newly developed crossed-beam-type electron spectrometer that allows for automatic compensation of any variations in electron beam intensity and the target gas density.

## II. EXPERIMENT

### A. Electron spectrometer

The spectrometer used in this experiment has been described in detail previously [18,19], however a few modifications have been carried out since then, hence a brief description of the apparatus is given below. A schematic diagram of the spectrometer is given in Fig. 1. Basically, the spectrometer is of crossed-beam type, where the incident electron beam collides with the target gas beam orthogonally and the scattered electrons are analyzed in the plane of the incident electron beam. The incident electron beam is generated by a Zipf-type electron gun [20], capable of producing a steady beam of electrons in the energy range 25–500 eV. The beam diameter (profile) and the energy spread determined separately from different experiments are about 3 mm and 300 meV, respectively. Beam currents ranging from few nA to few $\mu$A could be generated that is continuously monitored using a Faraday cup that reduces backscattering as well as suppress secondary electron emission and a calibrated electrometer (Keithley, Model-6514).

*bhushan@barc.gov.in

 ©2009 The American Physical Society

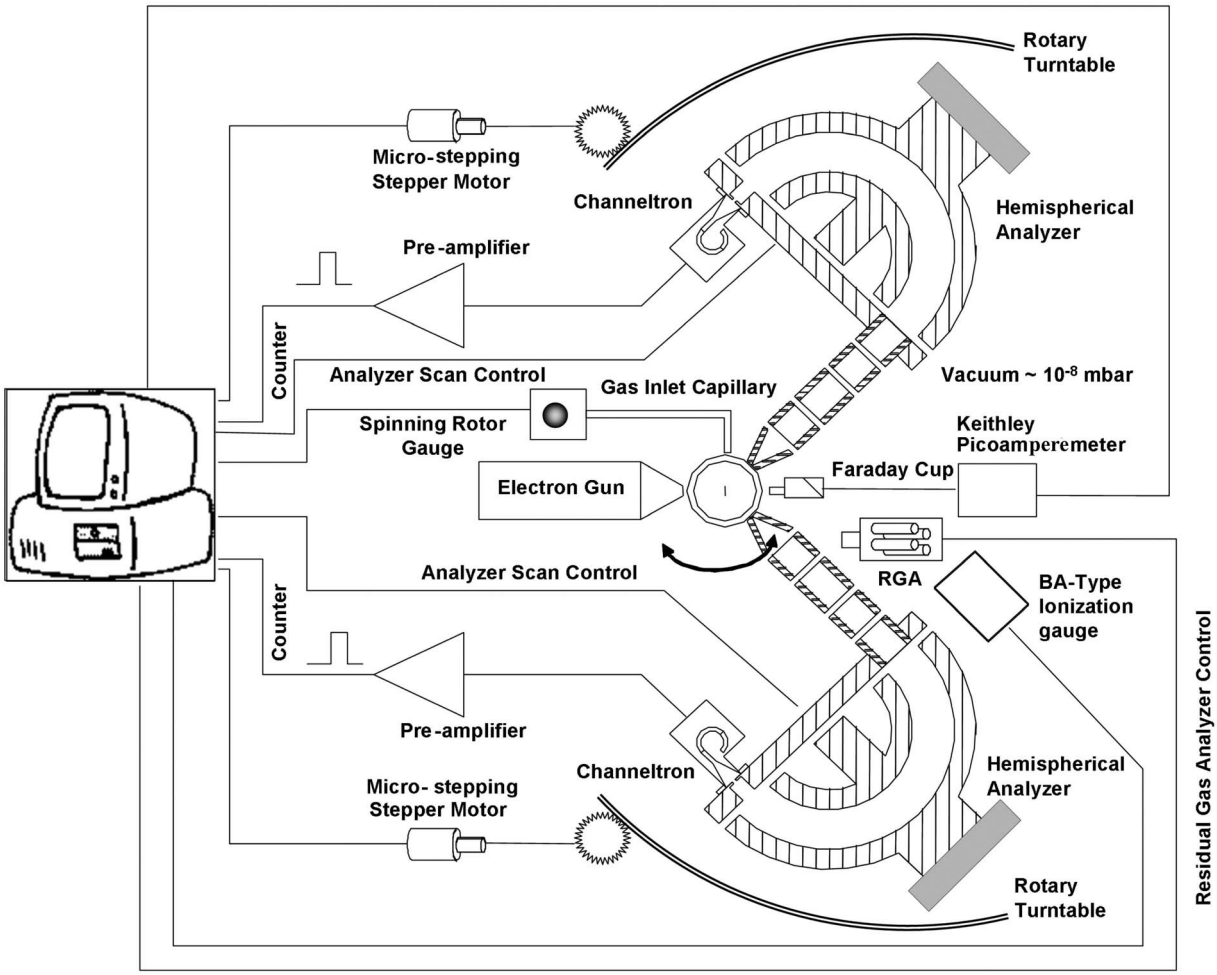


FIG. 1. Schematic diagram of the experimental setup.

The target gas is introduced through a mono-channel capillary 40 mm long, 0.22 mm internal diameter and a spinning rotor gauge (SRG 2CE, MKS Instruments GmbH, Germany) calibrated for the particular gas with traceability to international standards is used to measure the absolute pressure behind the inlet of the capillary tube. The flow rate is accurately measured with a calibrated automatic flow control meter (EVR 116 with RVC 300, Pfeiffer Vacuum, Germany). Typical number densities of the target gas at the scattering center estimated from this data are in the range of $10^{12}-10^{14}$ molecules/cm$^3$ depending on the inlet pressure [18].

The scattered electrons are energy and angle analyzed with the help of two identical hemispherical analyzers (Kevan-type) [21] with small solid angles (0.005 Sr) that image the entire collision region on to the exit plane of the hemispherical analyzer. This is achieved by coupling 5-element electrostatic zoom lenses before the entry plane of the hemispherical analyzer. Energy resolutions better than 0.2% of the incident energy (limited by the spread in the incident electron beam) have been achieved for all the energies used in this study. Channeltron multipliers mounted on the exit plane of the analyzers along with suitable pulse extraction and counting electronics are utilized to detect the scattered electrons after energy analysis. The analyzers are mounted on rotary turntables and can be rotated independently about the scattering center. Suitable microstepping stepper motors (with an angular repeatability of better than 0.1°) coupled to the shaft of a rotary vacuum feedthrough effect the rotation. The effective angular range is 120°, which is limited by the presence of the Faraday cup in the forward angles and the electron gun in the backward angles.

The entire spectrometer is kept in an ultrahigh vacuum chamber with suitable $\mu$-metal shielding that reduces the ambient magnetic fields to less than $10^{-6}$ T throughout the angular range of the analyzer. The chamber is pumped by a 500 l/s turbomolecular pump, which after sufficient baking produces a base pressure of about $2\times10^{-8}$ mbar. The background pressure increases by nearly 25 times to about $5\times10^{-7}$ mbar after the target gas has been introduced. A residual gas analyzer is utilized to measure the partial pressures of the background gases in the vacuum chamber. All experiments are conducted under steady-state conditions which are achieved by powering all electronic equipments for sufficiently long periods of time in order to eliminate any drift in power supplies during the measurement process.

### B. Experimental method

Absolute cross sections are obtained in a two-step process. In the first step, the relative cross sections are obtained

over the angular range ($\theta$=15°–135°) for a fixed incident energy using the normalized counting technique (described in the following section). In the second step, the absolute cross section is measured at one particular angle ($\theta$=30°) using the relative flow technique (described in the next sections) of Srivastava *et al.* [8] and later discussed by several authors [22,23], which is then utilized to convert the relative DCS into absolute elastic DCS.

#### *1. Measurement of relative cross sections*

In general, in crossed-beam type of experiments, the major source of uncertainty arises from the changes in scattering intensity due to fluctuations in the incident beam current ($\boldsymbol{I_o}$) and the target gas density ($\boldsymbol{n_T}$). Several methods have been utilized to overcome this problem and minimize the error in the overall cross-section data.

In the present experiment, two identical hemispherical analyzers with identical solid angles have been utilized (see Fig. 1). This is a unique feature of this experiment—the main advantage being, both analyzers image the same collision volume. One analyzer is kept fixed at $\theta$=30° while the other is rotated over the angular range. Since the scattered electron count rate is proportional to $\boldsymbol{I_o}$ and $\boldsymbol{n_T}$ and the scattering is isotropic about the electron beam, the fixed analyzer is used as a monitor for the product of $\boldsymbol{I_o}\cdot\boldsymbol{n_T}$. By performing angular distribution measurements on argon at two different energies (where a minimum is well known) the zero angle of the electron beam is determined.

All experiments were performed in the normalized counting mode. In the normalized counting technique, a preset number of counts are initially loaded in the fixed analyzer counter. Scattered electrons are counted in both the analyzers for the time it takes for the fixed analyzer to count down to zero. Thus any fluctuations in the incident current and the target gas density would be identically reflected in both the analyzers and automatically get normalized. This is possible only if both the analyzers image the same collision volume as is the case in our setup. All other parameters such as the flow rate ($\boldsymbol{Q_T}$), the partial pressure of the target gas ($\boldsymbol{p_T}$) in the vacuum chamber and the ambient pressure ($\boldsymbol{P}_{\mathrm{amb}}$) in the vacuum chamber are measured continuously. A background measurement was performed by closing the main leak valve and leaking in the same gas through a side port in the vacuum chamber such that the ambient pressure is equal to the ambient pressure when the target gas was flowing through the scattering center. Background counts are measured for the same time it took for the fixed analyzer to count down to zero from its preset value. These background counts are then subtracted from the scattered electron counts detected from true events. This gives the true counts for that particular angle and energy. The movable analyzer is rotated to the next angle and the procedure repeated.

The measured parameters can be related to the differential cross section as follows:

$$\left.\frac{d\sigma}{d\Omega}\right|_{(E,\theta)} = \frac{I_{\mathrm{sc}}(E,\theta) - I_B(E,\theta)}{I_0(n_T l \Delta_\omega)}\ \mathrm{cm}^2\ \mathrm{sr}^{-1}, \tag{1}$$

where, $I_{\mathrm{sc}}$ is the scattered electron current, $I_B$ is the background electron current, $I_0$ is the incident electron current, $n_T$ is the number density of the target gas beam, $\Delta_\omega$ is the solid angle subtended by the electron energy analyzers, and $l$ is the effective path length of the scattering region along the direction of the beam which is estimated from the overlap of the electron beam and the target gas beam profiles.

#### *2. Determination of absolute cross sections at 30°*

In order to put the relative cross sections on an absolute scale, a reference gas such as argon, whose absolute cross sections have been accurately measured for a particular energy ($E_o$) at a given angle ($\theta$) is utilized. In the relative flow technique any unknown cross sections for a gas can be determined by comparing the scattered electron currents with a gas whose cross section is well known at a particular angle, provided the angular distribution of the gas beam and the detection efficiency of the detector remain the same for both measurements.

It has been shown by Brinkmann and Trajmar [24], that the angular distribution of the gas beams will be the same if their Knudsen numbers ($K_n=\lambda/d$) (where $\lambda$ is the mean free path and $d$ is the diameter of the capillary) are equal as the gas enters the capillary channel.

The absolute cross-section measurements were conducted as follows. The absolute gas pressure behind the capillary is measured with a calibrated spinning rotor gauge and hence $\lambda$ can be calculated accurately. Argon is used as the calibration standard for which the cross sections have been accurately measured [25–27]. In the first instance the cross sections for argon at 30° were measured and equated to the already measured values. Then the Knudsen numbers for the gases under study are set to identical values as the calibration standard (in our case argon) and the corresponding scattered electron currents are measured. Counts are measured in the normalized counting mode ensuring a statistical accuracy better than 1%. A similar procedure was employed for determining the background counts as well. Under these conditions, the absolute cross section for the gas under study can be given as [28]

$$\sigma_g(E_o,\theta) = \sigma_c(E_o,\theta)\frac{N_c I_{oc}\sqrt{m_c}}{N_g I_{og}\sqrt{m_g}}\frac{I^s_{og}(E_o,\theta)}{I^s_{oc}(E_o,\theta)}, \tag{2}$$

where, $N_c$ and $N_g$ are the flow rates measured directly, $I_{oc}$ and $I_{og}$ are the incident electron currents during the respective measurements, $I^s_{oc}$ and $I^s_{og}$ are the scattered electron currents, $m_c$ and $m_g$ are the molecular masses and $\sigma_c$ and $\sigma_g$ are the elastic cross sections of the calibration standard and the gas under study, respectively.

The absolute cross section so determined at 30° is used to normalize the relative differential cross section to the absolute scale. A standard least-squares fitting function based on tenth-order Legendre polynomial expansion of the form

$$y = \sum_{n=0}^{10} a_n x_n, \tag{3}$$

where $x_n=P_n(\cos\theta)$ is the $n$th-order Legendre polynomial and $a_n$ are the fitting coefficients, is used to extrapolate the cross sections to 0° and 180°. The fitting curve was gener-

ated by using the curve fitting tool in MATLAB 6.5 software by giving the experimental data as input. From this data, the integral and momentum transfer cross sections are obtained.

### C. Error analysis

The largest single source of error in these measurements is the calculation of the number density of the target gas or in other words the ratio of the flow rates for the gases under study. Since the flow control meter was not calibrated for all gases, calibration to the nearest available mass number was selected. In order to reduce this uncertainty, the absolute pressure at the reservoir was also measured simultaneously, from which the number density could be estimated. The flow control meter and the absolute pressure measurement gauge are calibrated to better than 5% each. Thus from this data, it is estimated that the error in cross section due to the error in the flow rates to be less than 10%. Other errors arising due to counting statistics (<2%), measurement of electron beam current (<2%), gas pressure (<2%), and angular inaccuracy (<2%) are minimal. Further the spectrometer was also checked separately for multiple scattering effects by measuring the angular distributions at two different pressures of the target and confirmed that there was no qualitative change in the angular distribution. Errors in the absolute cross sections of the gas (in our case argon) used as the calibration standard also add to the overall error. Thus the overall errors in the differential cross sections mentioned in this study for $SF_6$ are about 12%. The integral and momentum cross sections have slightly larger errors due to the extrapolation procedures employed to extract the DCS at 0° and 180°.

In the case of $CS_2$, several "freeze-pump-thaw" cycles were performed to remove other gases that may be present since $CS_2$ is a liquid at room temperature with a vapor pressure of about 265 mbar. The error due to additional atmospheric gases present in the measurement cannot be ruled out. In order to minimize this possibility, the $CS_2$ container was kept warm at about 40 °C throughout the measurement increasing the vapor pressure of $CS_2$ to nearly atmospheric pressure. Nevertheless, an additional error of the order of 2% is estimated in the $CS_2$ cross sections due to the presence of other gases at the interaction region. Thus, the overall errors in the differential cross sections mentioned in this study for $CS_2$ are about 15%. (Note: $CS_2$ is a foul smelling "sticky," toxic gas that readily sorbs on the walls of the vacuum chamber. It is advisable to bake the vacuum chamber at high temperatures after the experiment and desorb the gas thoroughly prior to opening the vacuum chamber.)

## III. THEORY

The differential cross section (DCS) averaged over all possible orientations of the molecular axis as predicted by independent atom model (IAM) is given by [2,29]

$$I_{\mathrm{mol}}(\theta) = \sum_{a=1}^{N} I_a + \sum_{b\neq a}^{N} f_b^*(\theta) f_a(\theta) \frac{\sin Kr_{ab}}{Kr_{ab}}, \tag{4}$$

where $I_a$ is the atomic DCS of individual atoms present in the molecule, $K=2k\sin\frac{\theta}{2}$ is the magnitude of momentum transfer during the collision, $r_{ab}$ is the distance between the $a$th and the $b$th atom, $N$ is the total number of atoms in the molecule, $f_a(\theta)$ is the scattering amplitude of $a$th atom, and $k=\sqrt{2E}$ is the magnitude of the incident momentum vector of electron of energy $E$. In the case of $CS_2$, the above equation reduces to

$$I_{\mathrm{mole}} = I_{\mathrm{C}} + 2I_{\mathrm{S}} + 4(f_{\mathrm{S}}f_{\mathrm{C}} + f_{\mathrm{S}}^* f_{\mathrm{C}}^*)\frac{\sin Kr_{\mathrm{CS}}}{Kr_{\mathrm{CS}}} + 2f_{\mathrm{S}}^* f_{\mathrm{S}}\frac{\sin Kr_{\mathrm{SS}}}{Kr_{\mathrm{SS}}}, \tag{5}$$

where, $r_{\mathrm{CS}}=2.94a_0$ [30] is the distance between the carbon and sulphur atom and $r_{\mathrm{SS}}=5.88a_0$ is the distance between the two extreme end sulphur atoms, $a_0=0.529$ Å (Bohr radius), $f_{\mathrm{S}}, f_{\mathrm{S}}^*$ are real and imaginary scattering amplitudes of sulphur and $f_{\mathrm{C}}, f_{\mathrm{C}}^*$ are real and imaginary amplitudes of carbon, respectively. The scattering amplitude is calculated using the formula

$$f(\theta) = \frac{1}{k}\sum_{l=0}^{l_{\max}} (2l+1)(e^{i\delta_l}\sin\delta_l)P_l(\cos\theta), \tag{6}$$

where $P_l(\cos\theta)$ is Legendre polynomial of order $l$, $\delta_l$ is the $l$th-order phase shift of partial wave obtained from the NIST database [31] by numerically solving the radial Schrödinger equation

$$\left(\frac{d^2}{dr^2} + k^2 - V(r) - \frac{l(l+1)}{r^2}\right)u_l(r) = 0, \tag{7}$$

where, $V(r)=V_S(r)+V_{\mathrm{Exch}}(r)$. Here, $V_S(r)$, $V_{\mathrm{Exch}}(r)$ are static and exchange potentials for electron-atom interactions, respectively. The polarization potential is not included in the NIST calculations, hence we do not expect that the IAM predicts the correct theoretical cross sections at energies less than 100 eV. Even at energies higher than 100 eV, the above-mentioned IAM model calculations are purely used as a guide to understand the qualitative behavior of the differential cross sections in the present investigations.

## IV. RESULTS AND DISCUSSION

### A. Differential cross sections for $SF_6$

Figures 2(a) and 2(b) show the elastic DCS measured for $SF_6$ at different incident electron energies. Data from this experiment are compared with other similar data from previous experiments wherever available. At 50 eV the present experimental data agrees well with Johnstone and Newell [9] while there is a deviation from the data of Cho *et al.* [11]. The deviation is more noticeable in the backward angles. Another important feature is the sharp minimum around 75°. Our angular resolutions and the repeatability of angle measurement are better than 0.1°. Angular anisotropy is also negligible. It is surprising that the previous experiments have not given any evidence of such a sharp minimum as is seen in our experiment. In the case of 75 eV, the data agrees well with Cho *et al.* [11] both in forward as well as backward angles. The steep rise in the cross sections in the forward angles and the shoulder at around 25° is clearly noticed.

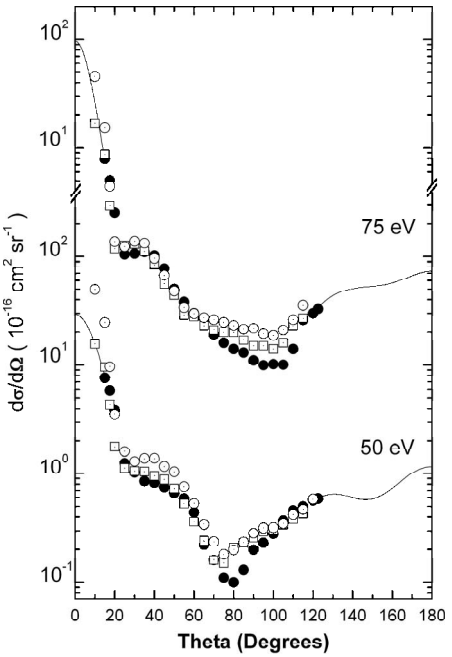


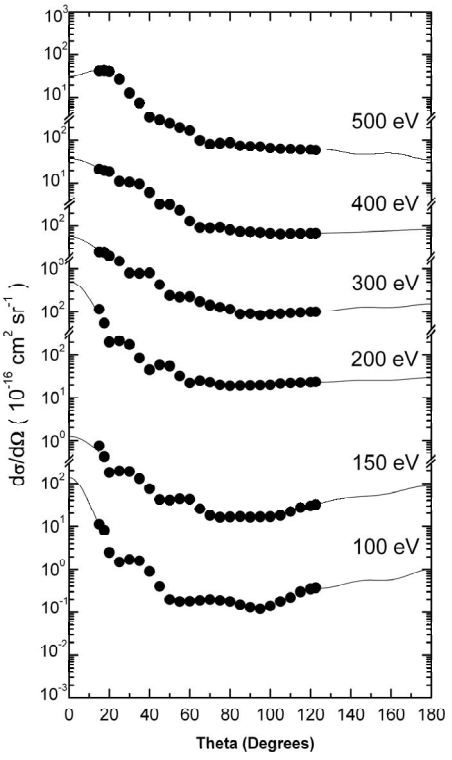


FIG. 2. (a) Elastic differential cross sections for $SF_6$ at incident energies 50 eV and 75 eV; ●, present experiment; ⊡, Johnstone and Newell [9]; ⊙, Cho *et al.* [11]. (b) Elastic differential cross sections for $SF_6$ at various incident energies from 100 eV to 500 eV.

However, at backward angles the cross sections seem to level off and no clear minimum is noticeable. At energies above 75 eV the only other measurement is that of Sakae *et al.* [10]. Our measurement agrees fairly well with this measurement within the prescribed error limits. Integral and momentum transfer cross sections are shown in Fig. 3. The overall errors in the Integral and momentum transfer cross sections are of the order of 20% and 25%, respectively, mainly due to the extrapolation of the data in the forward and backward angles.

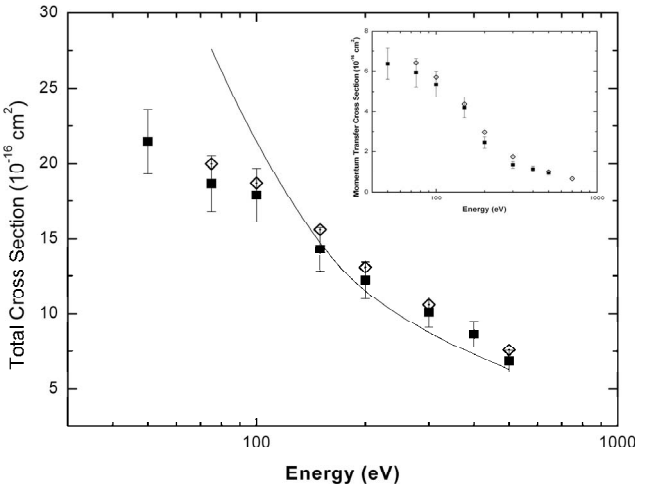


FIG. 3. Total cross section for electron-$SF_6$ scattering at various incident energies; ■, present experimental data; ♢, Sakae *et al.* [10]; and solid line is theoretical calculation from Joshipura [32]. Inset shows the momentum transfer cross section at various incident energies.

### B. Differential cross sections for $CS_2$

Figure 4(a) shows the measured absolute elastic differential cross sections for $CS_2$ at energies between 30 eV and 150 eV. No experimental data is available at these incident energies. At energies 50 eV and 100 eV, the experimental data are compared with the theoretical results from other groups. At 50 eV our experimental values are slightly higher than the theoretical values of Lee *et al.* [15] while at 100 eV the experimental data is fairly consistent with the theoretical values from the same group. The overall shape of the angular distribution is well represented. At 50 eV it is evident that there is a shift in the position of the minimum in the angular distribution as measured by our experiment and the theoretical calculations. It is conjectured that, since at low energies the de Broglie wavelength of the incident electron is comparable to or greater than the internuclear distance of the target molecule, a temporal reorientation of the charge cloud in the valence orbital takes place leading to a valence bond distortion effect. Thus a calculation incorporating valence bond distortion effects is required to understand the overall behavior of the angular distribution at low energies. However such a calculation is beyond the scope of the present investigations.

Figure 4(b) shows the measured absolute elastic differential cross sections for $CS_2$ at energies between 200 eV and 500 eV. Theoretical calculations based on the independent atom model as mentioned in the preceding section have been performed for energies above 100 eV. It can be seen that the theoretical calculations overestimate the cross sections throughout the angular range of the present measurements.

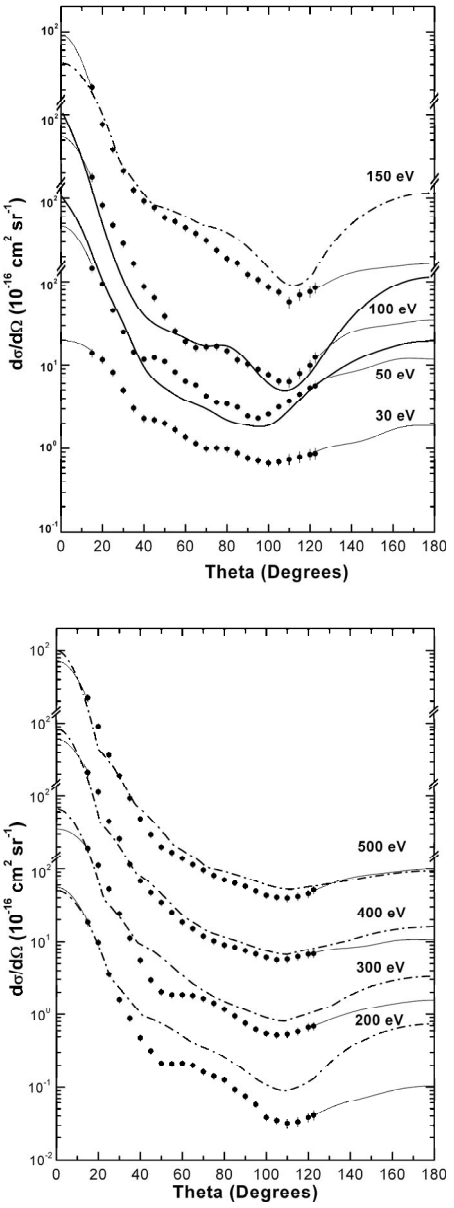


FIG. 4. (a) Elastic differential cross sections for $CS_2$ at incident energies between 30 and 150 eV. The thin solid lines on either side of the data points are the extrapolations based on the Legendre polynomial fitting as given in the text. The thick solid lines for 50 eV and 100 eV are theoretical calculations of Lee *et al.* [16] while the dashed-dotted line for 150 eV is theoretical calculation based on the IAM model given in the text. (b) Elastic differential cross sections for $CS_2$ at incident energies between 200 and 500 eV. The thin solid lines are the extrapolations based on Legendre polynomial expansions and the dashed-dotted lines are theoretical calculations based on the IAM model as given in the text.

$CS_2$ is a rotationally symmetric linear molecule with no permanent dipole moment and has only a quadrupole moment [33]. It remains unresolved whether this quadrupole moment needs to be incorporated in the theoretical treatment of the electron interaction with $CS_2$ along with the polarization term in order for correct calculation of cross sections. Thus at present, only the qualitative behavior of the angular distribution is explained. At energies above 300 eV, the simple

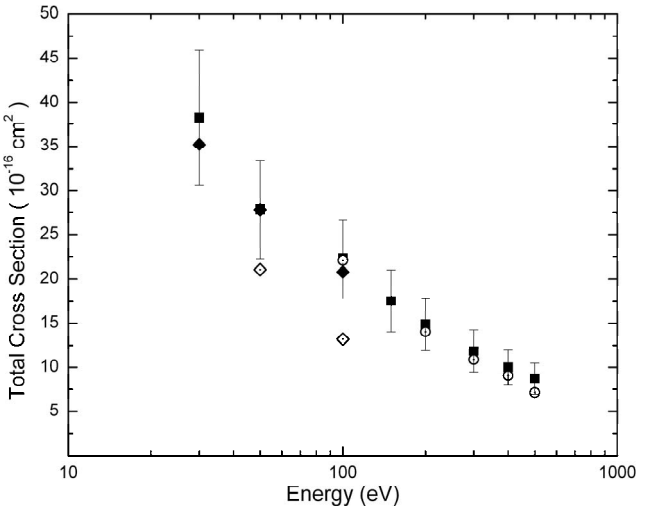


FIG. 5. Total (elastic plus rovibrational excitation) cross sections for $CS_2$ at various incident energies, ■ are the present experimental data; ◆, Szmytkowski [15]; ◇ and ⊙ are the theoretical values from Lee *et al.* [16] and Raj and Tomar [17], respectively.

IAM calculations with partial waves agree reasonably well with the experimental data.

Figures 5 and 6 show the integral and momentum transfer cross sections calculated from the present experimental data by extrapolating the data in the forward and backward angles. Data obtained for various incident energies are compared with other experimental or theoretical data wherever available. The resolution of the present experimental setup is insufficient to distinguish purely elastic from rovibrational excitation scattering. Hence it is possible that the measured cross sections could include a small contribution from rovibrational excitation cross sections also. The errors are higher in the integral and momentum transfer cross sections than the differential cross sections mainly due to the legendre polynomial extrapolations in the forward and backward angles.

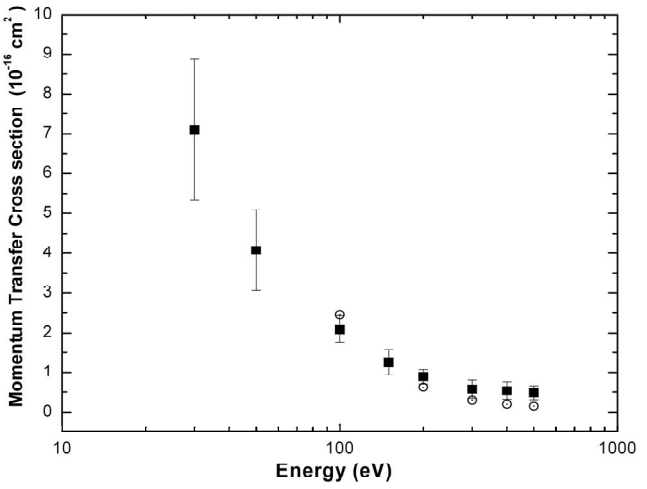


FIG. 6. Momentum transfer cross sections for $CS_2$ at various incident energies, ■ are the present experimental data and ⊙ are the theoretical values from Raj and Tomar [17].

Thus, the overall errors in the integral and momentum transfer cross sections are 22% and 27%, respectively.

## V. CONCLUSION

Elastic differential cross sections have been measured for electron scattering from $SF_6$ and $CS_2$ molecules using a crossed-beam-type electron spectrometer. The measured differential cross sections have been put on absolute scale using the relative flow technique. Cross sections for $CS_2$ in the intermediate energy regime are being reported for the first time. Integral and momentum cross sections obtained from the measured cross sections are compared with theoretical cross sections wherever available. At low energies there is a need to understand the qualitative behavior of the cross-section data using valence bond distortion theories, while at higher energies the IAM calculations describe the cross-section behavior adequately.

## ACKNOWLEDGMENTS

This work was supported by Department of Atomic Energy, Government of India, through project grant "Programme on Advanced Analytical and Other Instruments." The authors are grateful to Professor K. N. Joshipura, Department of Physics, Sardar Patel University, Vallabh Vidyanagar, Gujarat, India, for providing the theoretical total cross-section data for $SF_6$. Technical help of V. B. Chandratre for providing fast preamplifiers and electronics and S. M. Rodrigues for the assembly and alignment of the electron spectrometer is gratefully acknowledged.

[1] Winifred M. Huo and Yong-Ki Kim, IEEE Trans. Plasma Sci. **27**, 1225 (1999), and references therein.
[2] H. S. W. Massey, *Electronic and Ionic impact Phenomena*, (Oxford University, London, 1969), Vol. II.
[3] A. S. Dickinson, Astron. Astrophys. **54**, 645 (1977).
[4] A. Chutjian, Phys. Rev. Lett. **46**, 1511 (1981).
[5] N. Endo and Y. Kurogi, IEEE Trans. Electron Devices **ED27**, 1346 (1980).
[6] R. Pinto, K. V. Ramanathan, and R. S. Babu, J. Electrochem. Soc. **134**, 165 (1987).
[7] K. Rohr, J. Phys. B **12**, L185 (1979).
[8] S. K. Srivastava, S. Trajmar, A. Chutjian, and W. Williams, J. Chem. Phys. **63**, 2659 (1975).
[9] W. M. Johnstone and W. R. Newell, J. Phys. B **24**, 473 (1991).
[10] T. Sakae, S. Sumiyoshi, E. Murakami, Y. Matsumoto, K. Ishibashi, and A. Katase, J. Phys. B **22**, 1385 (1989).
[11] H. Cho, R. J. Gulley, K. W. Trantham, L. J. Uhlmann, C. J. Dedman, and S. J. Buckman, J. Phys. B **33**, 3531 (2000).
[12] Landolt-Börnstein, *Zahlenwerte und Funktionen* (Springer-Verlag, Berlin, 1951), Vol. I.
[13] G. L. Gustev and R. J. Bartlett, J. Chem. Phys. **108**, 6756 (1998).
[14] W. Sohn, K.-H. Kochem, K. M. Scheuerlein, K. Jung, and H. Ehrhardt, J. Phys. B **20**, 3217 (1987).
[15] C. Szmytkowski, J. Phys. B **20**, 6613 (1987).
[16] M. T. Lee, S. E. Michelin, T. Kroin, and E. Veitenheimer, J. Phys. B **32**, 3043 (1999).
[17] D. Raj and S. Tomar, J. Phys. B **30**, 1989 (1997).
[18] K. G. Bhushan, K. C. Rao, S. C. Gadkari, and J. V. Yakhmi, Bull. Ind. Vac. Soc. **9**, 13 (2006).
[19] K. C. Rao, K. G. Bhushan, S. C. Gadkari, and J. V. Yakhmi, Asian J. Phys. **16**, 353 (2007).
[20] P. Erdman and E. C. Zipf, Rev. Sci. Instrum. **53**, 225 (1982).
[21] S. D. Kevan, Rev. Sci. Instrum. **54**, 1441 (1983).
[22] S. Trajmar and D. Register, in *Electron-Molecule Collisions*, edited by I. Shimamura and K. Takayanagi (Plenum, New York, 1984).
[23] J. C. Nickel, C. Mott, I. Kanik, and D. C. McCollum, J. Phys. B **21**, 1867 (1988).
[24] R. T. Brinkmann and S. Trajmar, J. Phys. E **14**, 245 (1981).
[25] R. H. J. Jansen, F. J. de Heer, H. J. Luyken, B. van Wingerden, and H. J. Blaauw, J. Phys. B **9**, 185 (1976).
[26] S. K. Srivastava, H. Tanaka, A. Chutjian, and S. Trajmar, Phys. Rev. A **23**, 2156 (1981).
[27] G. G. Raju, IEEE Trans. Dielectr. Electr. Insul. **11**, 649 (2004), and references therein.
[28] I. Kanik, D. C. McCollum, and J. C. Nickel, J. Phys. B **22**, 1225 (1989).
[29] S. P. Khare, D. Raj, and Piyush Sinha, J. Phys. B **27**, 2569 (1994).
[30] G. Herzberg, *Molecular Spectra and Molecular Structure III. Electronic Spectra and Electronic Structure of Polyatomic Molecules* (Van Nostrand Reinhold, New York, 1966).
[31] A. Jablonski, F. Salvat, and C. J. Powell, NIST Electron Elastic-Scattering Cross-Section Database, Version 3.0, National Institute of Standards and Technology, Gaithersburg, MD, 2002.
[32] K. N. Joshipura (private communication).
[33] R. N. Compton, F. B. Dunning, and P. Nordlander, Chem. Phys. Lett. **253**, 8 (1996).